Chapter 10
Remote Sensing of Vegetation

Shin Nagai, Hideki Kobayashi, and Rikie Suzuki

10.1 Introduction

In eastern Siberia, interactions between terrestrial ecosystems above permafrost and the atmosphere affect global warming through their effects on carbon, water, and energy cycles. For instance, thawing permafrost produces continuous humid conditions, leading to forest degradation (Iijima et al. 2014), which reduces photosynthetic activity and thus the magnitude of the carbon sink, changes available water by decreasing evapotranspiration, and increases albedo, causing long-wave emissions to increase. The resulting increase in the thermokarst area may cause methane emission to increase (Flessa et al. 2008). Such increases in greenhouse gas emissions and albedo accelerate global warming. For an in-depth understanding of global climate change, it is essential to evaluate the spatiotemporal variability of ecosystem functions such as photosynthesis and evapotranspiration and ecosystem services (especially climate control) in eastern Siberia.

To evaluate the spatiotemporal variability of ecosystem functions and services, accurate observations of (1) aboveground biomass (stems, branches, and leaves), (2) plant functional type (PFT; e.g., deciduous coniferous or deciduous broad-leaved forest), and (3) growing season duration (i.e., the period from leaf-flush to leaf-fall) must be made over wide areas. These three parameters affect the carbon cycle through their effects on annual photosynthetic capacity and the carbon stock. Changes in PFT caused by climate change and human activities lead to changes in photosynthetic capacity, which in turn lead to changes in annual photosynthetic activity. Here, photosynthetic capacity refers to the maximum potential annual rate of photosynthesis and depends on leaf traits as well as the growing season duration (Wright et al. 2004; Richardson et al. 2013). In contrast, the annual gross primary production (GPP) reflects the actual rate of photosynthesis or photosynthetic activity

S. Nagai (✉) · H. Kobayashi · R. Suzuki
Japan Agency for Marine-Earth Science and Technology, Yokohama, Japan
e-mail: nagais@jamstec.go.jp

T. Ohta et al. (eds.), *Water-Carbon Dynamics in Eastern Siberia*,
Ecological Studies 236, https://doi.org/10.1007/978-981-13-6317-7_10

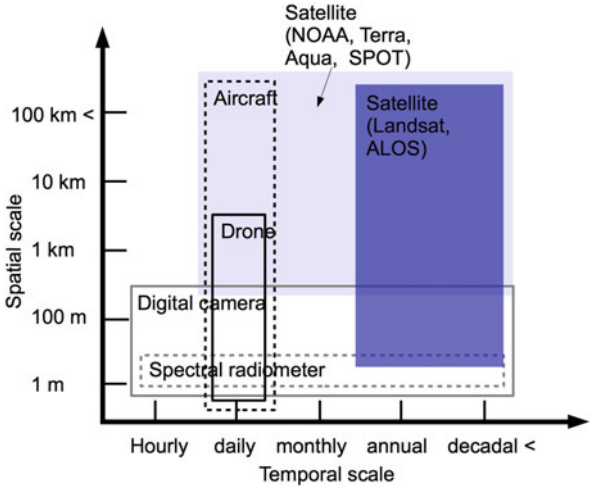

Fig. 10.1 Spatial and temporal scales of remote-sensing observations according to platform and sensor type

under daily weather conditions and is affected by long-term meteorological changes. Changes in photosynthetic activity cause changes in size of the annual carbon sink, which is determined by subtracting heterotrophic and autotrophic respiration from GPP, and in the amount of carbon (carbon stock) stored in stems and branches. Thus, mutual relationships among aboveground biomass, PFT, and growing season duration affect carbon flows and the carbon stock through their effects on photosynthesis.

Remote-sensing techniques, which use sensors such as digital cameras, spectral radiometers, and lasers mounted on platforms, including towers, drones, aircraft, and satellites, to observe targeted parameters from a distance, are useful means of obtaining data to evaluate spatiotemporal variabilities of aboveground biomass, PFT, and growing season duration (Fig. 10.1). The great advantage of remote-sensing techniques is that they make it possible to observe remote, mostly inaccessible areas, which are extensive in eastern Siberia. In this chapter, we review recent studies and discuss the use of remote-sensing techniques to observe terrestrial ecosystems in eastern Siberia. We focus on aboveground biomass, PFT, and growing season duration and how they affect interactions between terrestrial ecosystems and the atmosphere in the region.

10.2 Observation of Aboveground Biomass

Forest ecosystems in eastern Siberia play an important role in stabilizing the local and regional climate system through the surface energy transfer as evapotranspiration. Further, carbon assimilation by woody and soil ecosystem components helps to mitigate climate change through its effect on the global carbon cycle. Assimilated carbon in wood (i.e., forest biomass) generally represents the available biological resources. Remote-sensing techniques specifically detect the dry weight of the forest

biomass that is visible from satellites, that is, the aboveground biomass. The proportions of stems, branches, and leaves composing the aboveground biomass depend on the tree species. The allometric relationships between these components in Siberian larch (*Larix gmelinii*, *L. cajanderi*, and *L. sibirica*), a dominant tree species in eastern Siberia, and the total aboveground biomass have been studied by ground-based surveys (Kajimoto et al. 1999, 2006) at a limited number of field sites. Remote-sensing observations together with these allometric relationships can potentially be used to determine the spatial distributions over all of eastern Siberia of not only total aboveground biomass but also leaf biomass, the distribution of which must be known to estimate photosynthesis by the forest canopy.

10.2.1 Vegetation Indices

In satellite remote-sensing applications, vegetation indices have been widely used as proxies for aboveground biomass since the 1970s. One commonly used vegetation index is the normalized difference vegetation index (NDVI), which is derived from red and near-infrared (NIR) surface reflectances observed from satellites, where NDVI = (NIR − red)/(NIR + red) (Tucker 1979). NDVI, which typically takes a value between 0 (bare soil) and 1 (fully vegetated surfaces), is an indicator of the "amount of vegetation" and thus is closely related to biomass. High NDVI values imply large amounts of vegetation and abundant aboveground biomass (Fig. 10.2).

The effects of Arctic warming on the dynamics of boreal forests, including the forests of eastern Siberia, have been investigated by using NDVI data obtained by satellite-borne sensors. The Advanced Very High Resolution Radiometer (AVHRR) onboard National Oceanic Atmospheric Administration (NOAA) earth-observing satellites (hereafter NOAA-AVHRR) observed global vegetation dynamics from the 1980s to the 2000s (e.g., James and Kalluri 1994; Pinzon and Tucker 2014). Global analyses of NOAA-AVHRR data ($NDVI_{AVHRR}$) have detected decadal-scale NDVI changes (Myneni et al. 1997a; Zhou et al. 2001). These remote-sensing studies have revealed lengthening growing seasons and increases in maximum summertime NDVI values across the northern high latitudes, including in the larch forests of eastern Siberia. These results suggest that the amount of vegetation in the northern high latitudes was increased by the warming trend during the last 20 years of the twentieth century. However, the trend toward increasing the amount of vegetation in response to Arctic warming may not be monotonic. Studies in Eurasia covering an analysis period extending to 2006 have reported that NDVI showed a consistent increasing trend only until 1997 (1.8×10^{-3} year^{-1}), after which it started to decrease (-1.3×10^{-3} year^{-1}, Piao et al. 2011). In eastern Siberia, in particular, although the precipitation has a long-term increasing trend between 1982 and 2006 (0.39 mm yr.$^{-1}$, Piao et al. 2011), the growing season precipitation was decreased by -3.19 mm yr^{-1} in the time period between 1997 and 2006. This decreasing trend after 1997 potentially caused the decrease in summer NDVI trend (Piao et al. 2011).

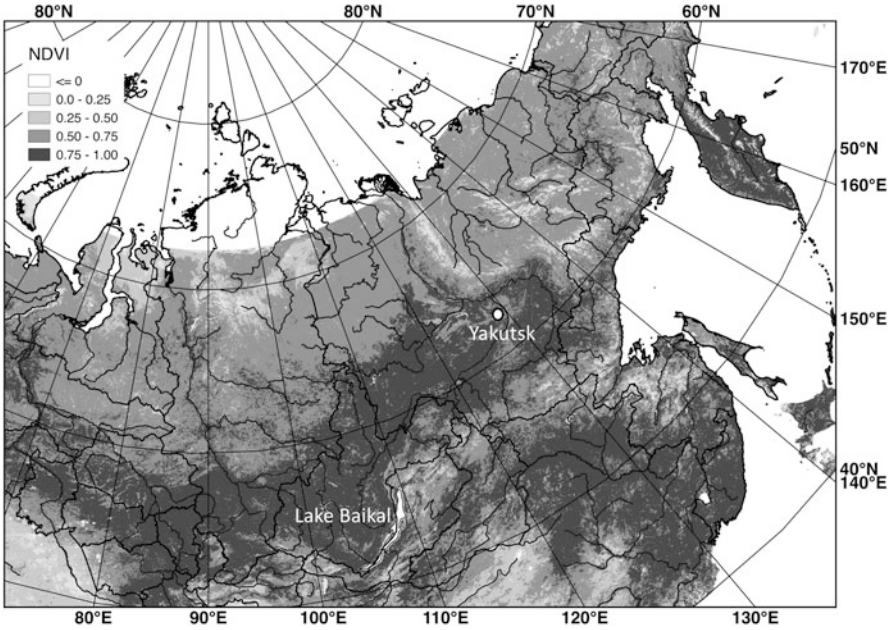

Fig. 10.2 NDVI distribution in eastern Siberia observed by SPOT-VGT in July 2010. The Russian political boarders are shown in bold lines. Rivers are shown in gray lines. White area shows higher NDVI values. Yakutsk is located in the middle of Lena River, and the NDVI values around the city of Yakutsk are higher than other regions

Although satellite-based NDVI is an effective way to investigate at large scale the duration of the forest growing season and the magnitude of vegetation changes, its interpretation is limited in several ways, particularly because changes in atmospheric conditions affect the monitoring results. For example, large-scale forest fires, which occur frequently in eastern Siberia, enhance aerosol loading in the atmosphere, and the presence of more aerosols in the atmosphere may cause the NDVI to decrease, even though no actual change in the vegetation status has occurred. In addition, cloud cover above eastern Siberia often prevents detection of vegetation signals. Most satellite NDVI data are processed by applying a maximum-value compositing procedure to extract the best NDVI values obtained during a specified time period and using those values to create the NDVI product. $NDVI_{AVHRR}$ products often use time periods of 10 days. If no days during a 10-day period are clear, then the highest NDVI value is selected regardless of cloudiness. Because the sky in many parts of eastern Siberia is likely to be cloud covered for periods exceeding 10 days, some NDVI values are affected by clouds.

Furthermore, NDVI values can depend on the data processing procedures that have been applied, such as sensor-related geometric and radiometric corrections, atmospheric correction schemes, and post-processing schemes (gap filling, compositing). Thus, to interpret the NDVI trends accurately, multiple data sets

should be compared to better understand the nature of the vegetation signal. These limitations are further described in Sect. 10.4.2.

NDVI is often used as an indicator of "vegetation greenness" or the "amount of vegetation," but these parameters do not directly correspond to any forest structure parameters. However, to the extent that aboveground biomass is related to leaf biomass, NDVI also correlates with leaf biomass. The aggregate $NDVI_{AVHRR}$ throughout the growing season is significantly correlated with ground-based measurements of the aboveground biomass of diverse tree species across boreal and temperate forests, and the relationship obtained by regression analysis between NDVI and aboveground biomass can be used to quantify the large-scale geographical distribution of aboveground biomass (Myneni et al. 2001). It must be noted that, unlike synthetic aperture radar (SAR), which can be used to estimate aboveground biomass more directly (see Sect. 10.2.3), NDVI-based biomass estimation is an indirect approach, because NDVI is sensitive mainly to leaf biomass rather than to total woody biomass. Thus, the interpretation of biomass data derived from NDVI data has inherent uncertainty.

10.2.2 Leaf Area Index

Among the three major aboveground biomass elements, leaf biomass, trunk biomass, and branch biomass, leaf biomass is the one important for characterizing forest canopy photosynthesis and thus productivity. In terrestrial biogeochemical models, leaf biomass is often represented by the leaf area index (LAI), which is defined as the one-sided leaf area per unit of ground area ($m^2\ m^{-2}$). LAI is derived by dividing the leaf biomass (g m^{-2}) by the leaf mass per unit of leaf area (leaf mass area, LMA; g m^{-2}). When the forest LAI is larger, the amount of sunlight intercepted by leaves increases, thus enhancing canopy-scale photosynthesis. The typical LAI of a forest ecosystem varies greatly, depending on the tree species, climate, topography, and soil water and nutrient conditions. In eastern Siberia, most forests are sparse, and the maximum LAI in summer is less than 4 (Kobayashi et al. 2010). The actual LAI varies spatially over eastern Siberia; however, so to evaluate forest ecosystem carbon dynamics, the regional LAI distribution must first be determined. Because the ground-based measurements cannot cover the whole area, remote-sensing observations are essential for producing regional distribution maps of LAI in eastern Siberia.

Two remote-sensing methods are used to produce regional- to global-scale LAI distribution maps. The first method, the so-called vegetation index-based method, is based on the biome-specific regression relationships between NDVI and LAI. Once the NDVI–LAI regression relationship is determined, it can be applied to satellite NDVI data sets to map LAI across eastern Siberia. NDVI is computed from the red and NIR spectral reflectances (e.g., red, 0.58–0.68 μm, and NIR, 0.725–1.00 μm for NOAA-AVHRR; see Sect. 10.2.1). Red reflectance is sensitive to the total chlorophyll content of the canopy, and NIR, which results from multiple scatterings within the canopy, is sensitive to the quantity of leaves. The chlorophyll content of the

forest canopy increases as LAI increases. As a result, more red sunlight is absorbed by the leaves, and the red reflectance decreases. Because no pigments absorb sunlight in the NIR spectral domain, when LAI increases, sunlight is reflected by or transmitted through the leaf surfaces many times, enhancing the NIR reflectivity of the forest canopy surface. These distinct features of the red and NIR spectral domains explain why NDVI increases when LAI increases (e.g., Myneni et al. 1997b). Once the NDVI and LAI relationship is determined from field measurements of LAI and red and NIR spectral reflectances, the relationship can be applied to large-scale mapping of LAI. The vegetation index method (NDVI–LAI relationship) is easy to apply to various forests once the NDVI–LAI relationship for the specific forest types such as an open needleleaf forest is determined. However, because of differences in forest structure, spatial leaf distribution (clumping), and leaf-angle distribution, a single LAI value may be associated with several NDVI values, which is a limitation on the accuracy of the LAI values retrieved by using this simple empirical approach.

The second method uses a sophisticated forest canopy radiative transfer model for inverse estimation of LAI from satellite-observed spectral reflectances. The improved accuracy of the surface spectral reflectances retrieved by the VEGETATION sensor onboard the French satellite SPOT (hereafter SPOT-VGT), which was launched in 1998, and the Moderate Resolution Imaging Spectroradiometer (MODIS) sensor onboard the US National Aeronautics and Space Administration (NASA) satellite Terra (hereafter Terra-MODIS), compared with NOAA-AVHRR data, allows LAI to be estimated by using a physically based radiative transfer model inversion approach (Knyazikhin et al. 1998). For example, canopy total LAI for application to climatic and vegetation dynamics studies has been operationally mapped, including in eastern Siberia, with spatial resolutions of 500 m to 1 km by using Terra-MODIS data acquired every 4–8 days since 2000 by the NASA MODIS science team (Myneni et al. 2002, Fig. 10.3). Canopy LAI maps from Terra-MODIS and SPOT-VGT are useful for studying eastern Siberia as a whole, though a regional-scale study might need a higher-resolution data set. In this regard, the Landsat series satellites provide reflectance images with a spatial resolution of 30 m. By using Landsat data, a detailed map of LAI in a specific area of eastern Siberia can be produced. For example, a LAI distribution map of the forest around the Lena River near the city of Yakutsk produced by radiative transfer model inversion (Kushida et al. 2007) shows that in larch forests on the left bank of the Lena River, LAI varies from 1 to 3 in the summer.

The dominant genus of trees in eastern Siberia is larch (*Larix gmelinii*, *L. cajanderi*, and *L. sibirica*), where it forms large forests, either as pure stands or in association with pine (*Pinus sylvestris*), spruce (*Picea obovata*), and other species. More than 50% of the total forested area in eastern Siberia (2.5×10^6 km^2) consists of larch forest. Most larch forests are sparse with a typical LAI of no more than 4. Therefore, a large amount of sunlight penetrates the larch canopy and reaches understory and forest floor plants. This light environment provides favorable conditions for forest floor species such as cowberry (*Vaccinium vitis-idaea*, a small shrub), mosses, and lichens. Because the floor of a larch forest is mostly covered by such

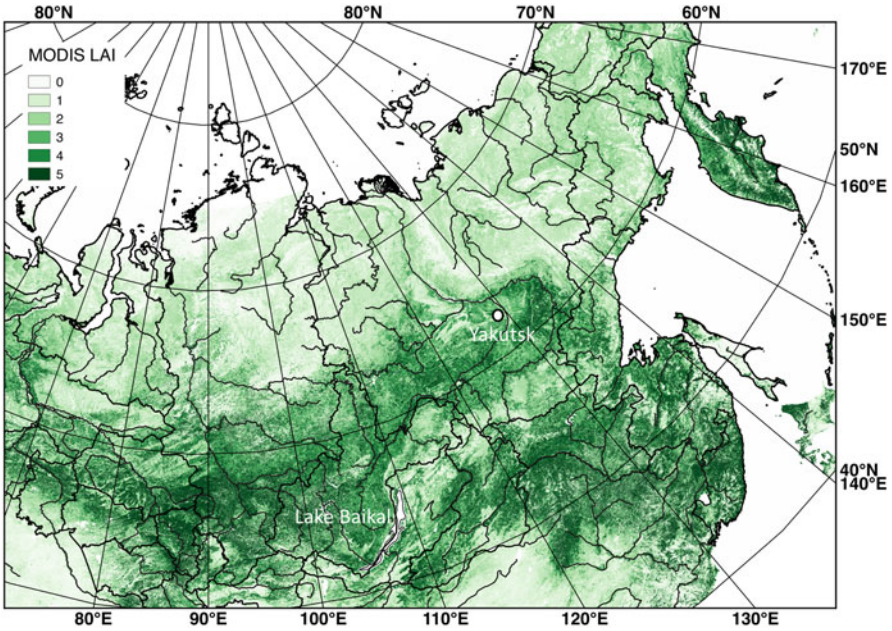

Fig. 10.3 LAI distribution in eastern Siberia estimated from Terra-MODIS data sets

plants, their contributions to photosynthesis and evapotranspiration of the forest as a whole are not negligible. Although the size of their contributions depends on the age of the forest stand, Iida et al. (2009) reported that more than 50% of total evapotranspiration from a larch forest near Yakutsk was attributable to the forest floor layer.

The contribution of the forest floor vegetation to photosynthesis and evapotranspiration can be evaluated by estimating the LAI of the larch overstory and the forest floor plants separately. Even though larch forests are sparse, satellites can rarely observe the forest floor vegetation in summer owing to the greenness of the larch canopy (Kobayashi et al. 2007). However, because larch is a deciduous needle-leaved tree, during early spring (after snow melt and before larch foliation), it is possible to monitor the forest floor vegetation by satellite (e.g., Kobayashi et al. 2010; Liu et al. 2017). Most forest floor plants such as cowberry are evergreen, so the seasonal changes in their LAI are small. Once the forest floor plants' signature which is related to the forest floor LAI is determined from springtime satellite data, then the LAI of the larch overstory can be estimated by using the forest floor information as background data. Under the assumption that the forest floor LAI is constant throughout the growing season, seasonal changes in satellite reflectance signals can be attributed to seasonal changes in the larch canopy. For example, Kobayashi et al. (2010) estimated the larch overstory LAI in Siberian larch forests from the seasonal increase in the normalized difference water index (NDWI) after snow melt, where NDWI = (NIR − shortwave infrared)/(NIR + shortwave infrared). The relationship

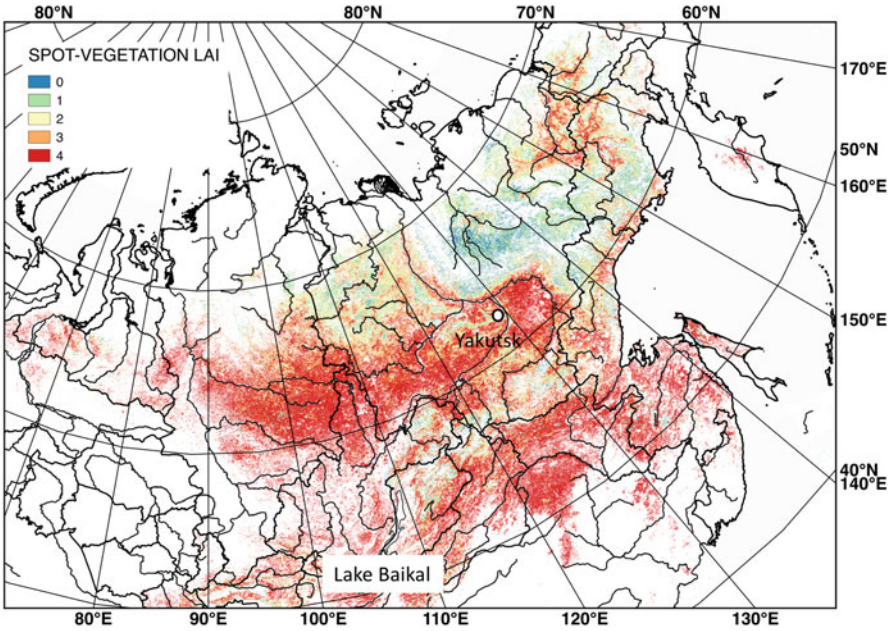

Fig. 10.4 Larch overstory LAI in eastern Siberia estimated from SPOT-VGT data sets

between increases in NDWI and LAI has been calibrated for various forest floor LAI data sets by using a radiative transfer model. The spatial distribution of the larch overstory LAI in eastern Siberia shows a distinct north–south gradient in summer (Fig. 10.4). In addition, LAI can vary along elevation; LAI is lower in the Stanovoy Mountains than in surrounding regions. The estimated LAI distribution is useful for validating the LAI distribution simulated by ecosystem models. For example, Sato et al. (2016) used satellite-based summer maximum (July) overstory LAI data averaged over 1998 to 2013 in order to validate the latitudinal gradient of simulated LAI at the present time (the year of 2005). The present study also estimated the geographical distribution of forest floor information that is related to the forest floor LAI (it was called as apparent forest floor LAI). However, the accurate quantification of understory LAI is one of the challenging parts because there are few field observations that are used for validation and calibration of the remote-sensing measurements.

10.2.3 Radar and LiDAR Remote Sensing

Microwave satellite remote-sensing techniques provide a different view of forest ecosystems. SAR is an active microwave radar technology commonly used in satellite remote sensing. SAR observations, for example, those of the Phased

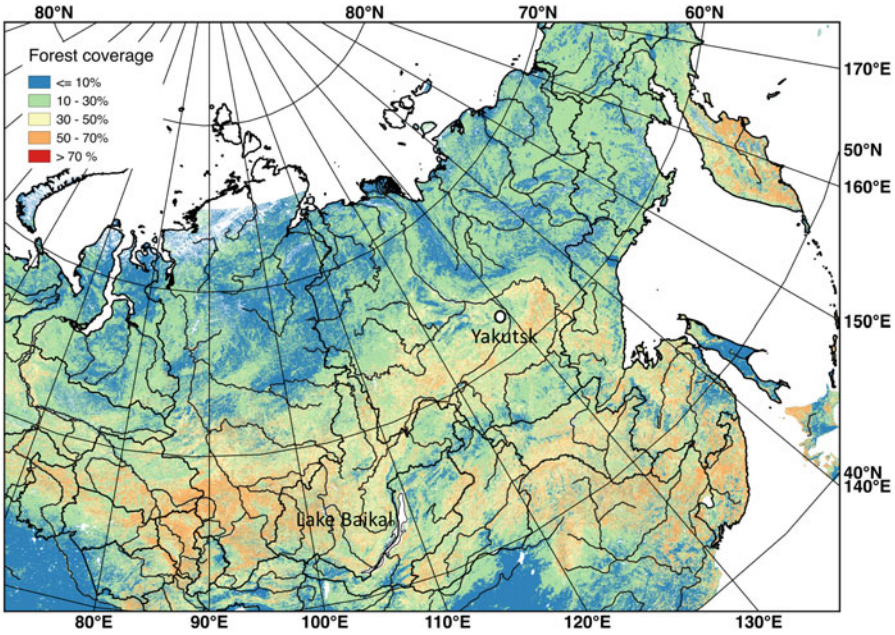

Fig. 10.5 Map of forested (black) and non-forested areas of eastern Siberia determined by using ALOS-2-PALSAR data sets

Array type L-band Synthetic Aperture Radar (PALSAR) onboard the Advanced Land Observing Satellite (ALOS), are particularly useful for distinguishing aboveground biomass between forested and other regions (Fig. 10.5). L-band microwaves with a wavelength of 23 cm, which penetrate the forest canopy and are scattered by tree trunks, a phenomenon called volume scattering, are particularly useful for estimating the aboveground biomass of the forest, because the returning backscattered L-band SAR signal is an indicator of the trunk biomass. When the aboveground biomass is relatively small, it can be estimated from SAR data merely by removing the micro-topographical effect. However, the backscattered SAR signal saturates as the aboveground biomass becomes higher.

The aboveground biomass can also be estimated by using canopy height information obtained by the satellite-based laser altimetry measurements. The Geoscience Laser Altimeter System (GLAS) onboard NASA's Ice, Cloud, and land Elevation Satellite (ICEsat), which was operational during 2003–2009, provided a global canopy height map with a spatial resolution of 1 km (Simard et al. 2011). In eastern Siberia, the forest canopy height in the middle basin of Lena River near Yakutsk reaches up to 30 m and higher than downstream regions in the high latitudes (Fig. 10.6), where LAI in the same region is also higher than other regions (LAI = 3–4; see Figs. 10.3 and 10.4).

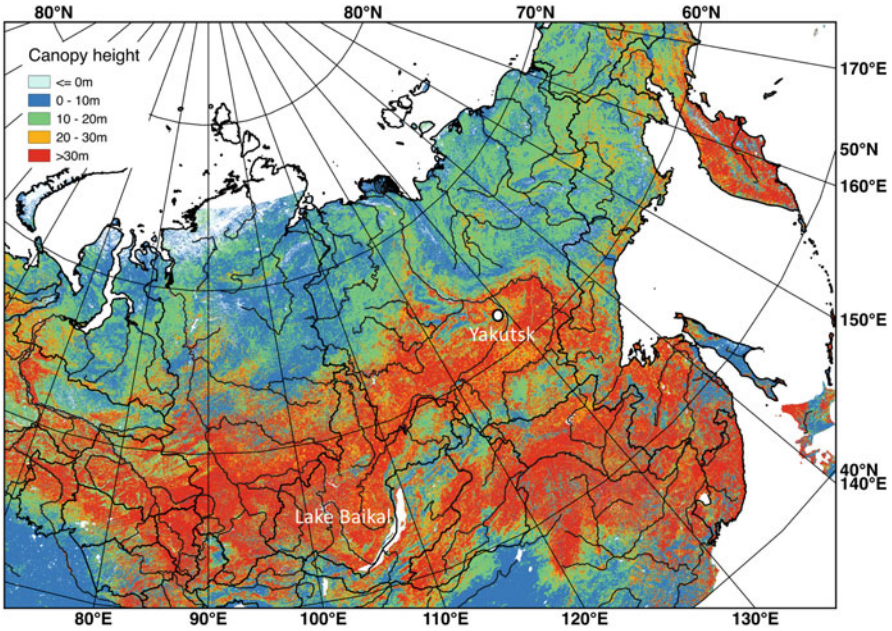

Fig. 10.6 Forest canopy height (m) distribution in eastern Siberia estimated from ICEsat-GLAS data sets

10.3 Observation of Plant Functional Type

Plant functional type (PFT) is a classification system for plant species and simplification of floristic complexity in global vegetation models (Prentice et al. 1992). Species-specific mapping of plants at a continental scale is not feasible, so PFT is mapped by first classifying the plant species in various regions according to plant traits. PFT maps compiled in this way are used as fundamental information on the ecosystem model simulation. PFT maps of eastern Siberia have been produced by Terra/Aqua-MODIS (MCD12Q; resolution 500 m) and the Medium Resolution Imaging Spectrometer (MERIS) onboard European Space Agency Envisat satellites (GlobCover2009; resolution 300 m). Suzuki et al. (2004) produced a detailed regional-scale PFT map from airborne observations of the area around the Lena River from April 24 to June 19, 2000. These regional maps show spatial patterns of larch on permafrost, evergreen needle-leaved species, and birch, as well as the spatial pattern of thermokarst features such as alases.

During long-term environmental monitoring, the temporal variability of PFT distributions must be taken into account. In eastern Siberia, large forest fires that burn canopy trees, forest floor vegetation, and soil organic matter occur on a decadal scale. Spatial and temporal variations of burned areas can be estimated by comparing satellite images acquired before and after fires. For example, in eastern Siberia, the burned area fraction in 0.25° latitude × 0.25° longitude grids was mapped by using

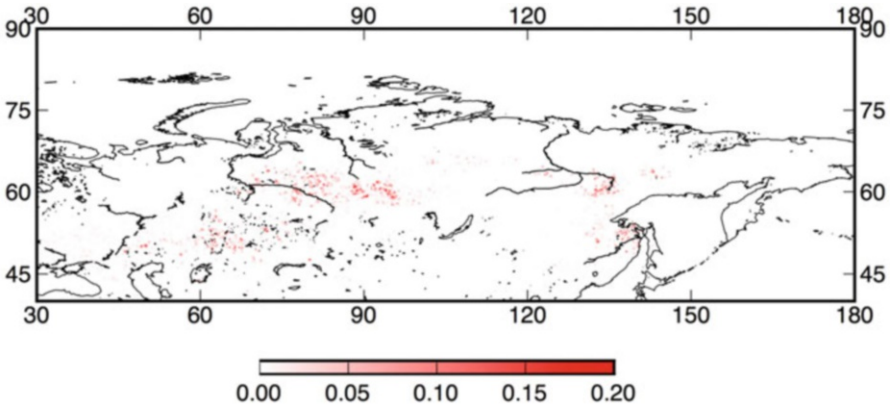

Fig. 10.7 Burned area fraction in eastern Siberia in July 2010 mapped by using data from the GFED

data from the Global Fire Emissions Database (GFED version 4.0; Giglio et al. 2013; Fig. 10.7). Such burned area maps are useful for monitoring not only forested area changes but also greenhouse gas and aerosol emissions (CO_2, CO, black carbon) from fires.

10.4 Observations of Growing Season Duration

10.4.1 Satellite Observation

AVHRR-NOAA, SPOT-VGT, and the MODIS sensors onboard Terra and Aqua (hereafter Terra/Aqua-MODIS), which observe the whole world at a daily time step, allow spatiotemporal variability in the timing of the start (SGS) and end (EGS) of the growing season to be detected. The $NDVI_{AVHRR}$ time series, which covers more than 30 years, is remarkable for its length, although there are some serious issues to be considered (see Sect. 10.4.2) (Buitenwerf et al. 2015). Buitenwerf et al. (2015) showed that the average of growing season duration from 2003 to 2012 became longer in boreal regions than that from 1981 to 1990. The average of timing of SGS from 2003 to 2012 became earlier than that from 1981 to 1990. In contrast, the difference between the average of timing of EGS from 2003 to 2012 and that from 1981 to 1990 showed spatial characteristics. In the northern areas, the average of timing of EGS became earlier. In the further south areas, the average of timing of EGS did not change. In the still further south areas, the average of timing of EGS became later. Delbart et al. (2006), who analyzed time series of $NDVI_{AVHRR}$ and SPOT-VGT-based normalized difference water index (NDWI) from 1982 to 2004, reported year-to-year variability in the spatial distribution of the timing of SGS in Siberia. The NDWI data have the advantage that they allow the timing of snow melt

to be distinguished from that of SGS. Their analysis also showed that from 1982 to 2004, the timing of SGS tended to occur earlier each year in Northeast Siberian taiga and areas from Lake Baikal toward Ob River's mouth, but they observed delayed trend in eastern Siberia (Yakutsk region).

Suzuki et al. (2001) examined the spatial characteristics of the relationships among $NDVI_{AVHRR}$, PFT, temperature, and precipitation. These relationships explain the spatial differences in the growing season duration in boreal ecosystems. Suzuki et al. (2007) showed that $NDVI_{AVHRR}$ was positively correlated with temperature and negatively correlated with precipitation in eastern Siberia. These relationships indicate that interannual changes in vegetation and the resultant interannual changes in evapotranspiration are controlled by temperature in the northern low-temperature region of eastern Siberia (Suzuki et al. 2007).

10.4.2 Satellite Observation Issues

Despite the usability of satellite remote-sensing observations, five issues remain that can cause uncertainty in the detection of the growing season in eastern Siberia as well as misleading results.

10.4.2.1 Issue 1: Systematic Noise

NOAA-AVHRR satellite data include systematic noise caused by satellite drift and large volcanic eruptions (Jin and Treadon 2003). The SPOT-VGT and Terra/Aqua-MODIS products have reduced systematic noise due to satellite drift, but no satellite sensors can eliminate systematic noise due to large volcanic eruptions.

10.4.2.2 Issue 2: Atmospheric Noise and Cloud Contamination

Satellite observations are affected by atmospheric noise (e.g., smoke and chemical emissions, yellow sand dust storms) and cloud cover. Motohka et al. (2011) showed that about 40% of satellite data observed by Terra-MODIS with cloud screening by the state flag of satellite product still included cloud contamination. In eastern Siberia, satellite observations are often affected by atmospheric noise due to haze and smoke from forest fires.

10.4.2.3 Issue 3: Heterogeneity of Plant Functional Type

PFT heterogeneity within single pixels of satellite data causes uncertainty in phenological observations. This uncertainty is larger in data from SPOT-VGT and Terra/

Aqua-MODIS, which have spatial resolutions of 1.1 km and 250 m, than in data from Landsat series satellites, with a spatial resolution of 30 m.

10.4.2.4 Issue 4: Effect of Solar Zenith and View Angles

In the high latitudes, the effect of solar zenith and view angles on satellite data also causes uncertainty in phenological observations (Kobayashi et al. 2016). Particularly in autumn (late August and September), the solar zenith angle becomes very high (over 60°), and in boreal forests, sunlight coming from an oblique direction is mainly reflected from the top of the canopy; the forest floor is rarely illuminated. As a result, even in a sparse forest, phenological information about forest floor plants from satellite observations is limited (Kobayashi et al. 2016).

10.4.2.5 Issue 5: Insufficient Ground-Truthing

Ecological interpretation of satellite data is difficult because the data are not yet sufficiently constrained by ground-truthing (Nasahara and Nagai 2015). In areas receiving heavy snowfall, in situ observations have shown that vegetation indices in spring reflect both melting snow and leaf-flush, and in autumn they reflect both leaf-fall and snowfall (Nagai et al. 2010). Confusion between phenological phenomena, leaf-flush and leaf-fall, and melting and falling snow in time series of satellite-observed vegetation indices produces misleading analysis results regarding the timing of SGS and EGS.

10.4.3 In Situ Observations

To resolve these problems, satellite remote-sensing observations must be validated by performing field studies with, for example, time-lapse digital cameras and spectral radiometers (Nasahara and Nagai 2015). Continuous observations of phenological phenomena such as leaf-flush, leaf-coloring, and leaf-fall by time-lapse digital cameras, along with measurements of CO_2 and H_2O fluxes and micrometeorological observations, have been carried out since June 2013 in a deciduous coniferous (larch) forest at the Spasskaya Pad Scientific Forest Station near Yakutsk in eastern Siberia (62°15′18”N, 129°37′08″E) (see Chap. 3). Time-lapse digital cameras (Coolpix-4300/4500, Nikon, Tokyo, Japan) were installed at heights of 32 m on a CO_2 flux tower and 3 m on the forest floor. The cameras acquire plant phenology images of the overstory (forest canopy) and understory vegetation (forest floor) every hour during the daytime (Nagai et al. 2018). This larch forest site is part of the Phenological Eyes Network (http://www.pheno-eye.org; Nasahara and Nagai 2015).

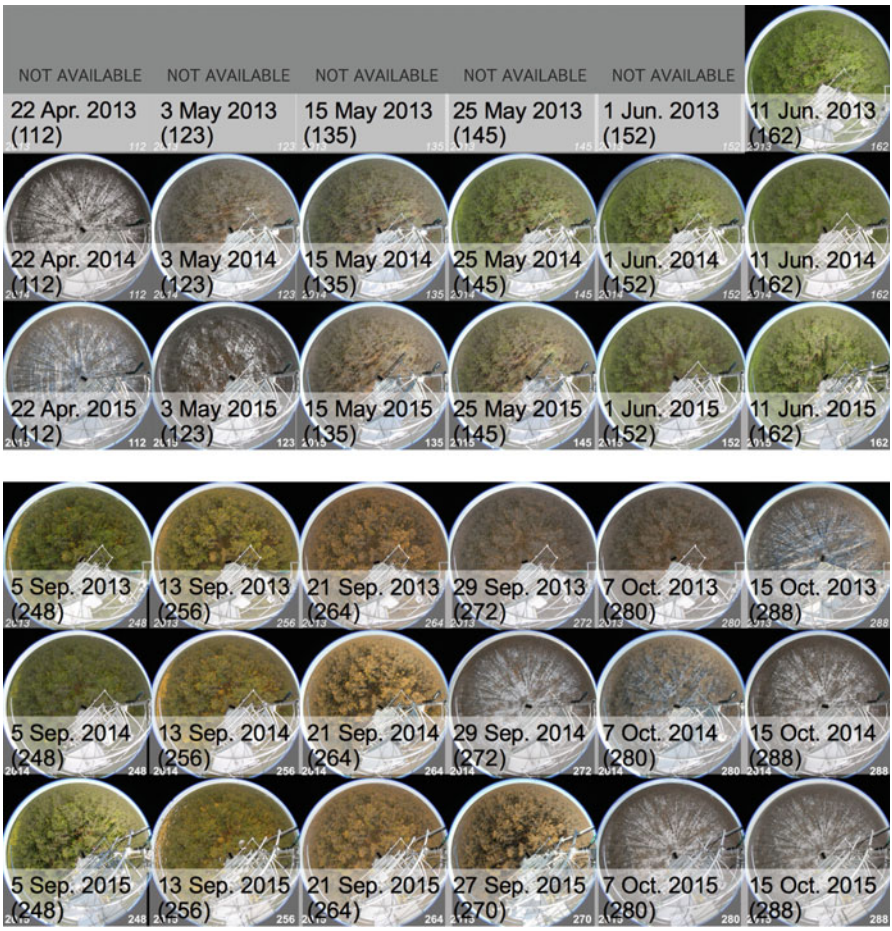

Fig. 10.8 Typical phenological images in spring (top) and autumn (bottom) of the Spasskaya Pad larch forest from June 2013 to June 2016. Date and day of year (in parenthesis) are shown on each phenological image

Typical phenological images of the Spasskaya Pad larch forest (Fig. 10.8) obtained over a 3-year period show the timing of phenological events: leaf-flush in larch during mid- to late May, leaf-coloring in birch from early to mid-September, and leaf-fall in larch from late September to mid-October. In addition, snow melt was imaged between late April and early May, and the first snowfall was observed between late September and early October. In birch, an understory component, leaf-flush occurred about a week later than it did in larch, which composes the overstory. In contrast, leaf-coloring was about a week earlier in birch than in larch. In larch, leaf-flush occurred 13 days earlier in 2014 than in 2015, and leaf-fall occurred about 10 days earlier in 2013 than in 2014 and 2015. Examination of the seasonal

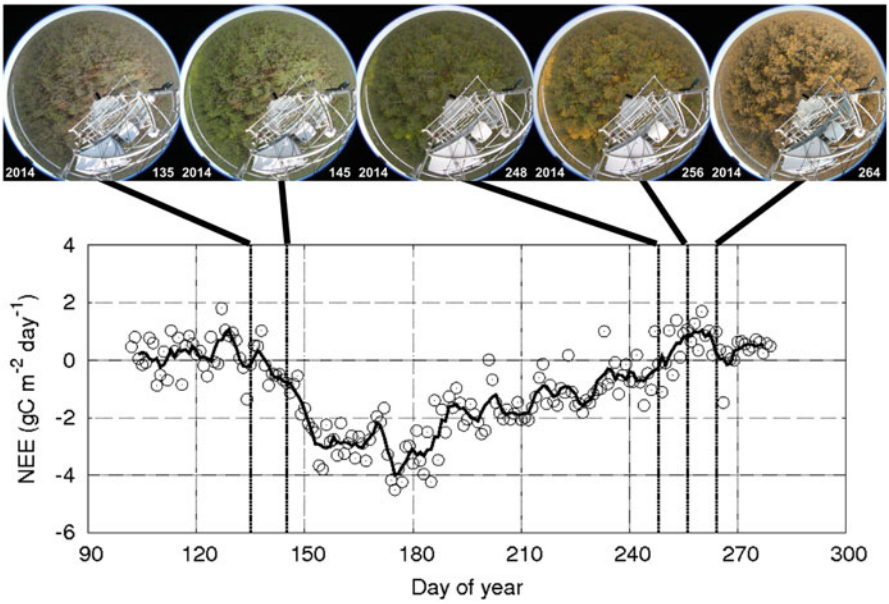

Fig. 10.9 Seasonal changes in flux-based NEE in 2014 (from Kotani et al. unpublished) in relation to typical phenological images of the Spasskaya Pad larch forest. The solid line shows the 5-day moving average

relationships between CO_2 flux-based net ecosystem exchange {NEE, where NEE = − [GPP – autotrophic (AR) and heterotrophic respiration (HR)]; see Chap. 4} and typical phenology (Fig. 10.9) showed that the first date on which NEE was less than zero in spring (i.e., the first date on which carbon absorption was greater than carbon emission) occurred just after leaf-flush in larch, whereas the first date on which NEE was more than zero in autumn occurred before both leaf-coloring in birch and leaf-fall in larch.

Long-term continuous phenological images are useful for detecting year-to-year variations in the timing of leaf-flush, leaf-coloring, and leaf-fall in each tree species as well as in the snow-covered period. However, visual inspection of phenological images is qualitative. Depending on the individual conducting the inspection, the timing of each phenological phenomenon can differ by as much as a few days. Phenological images consist of red (DN_R), green (DN_G), and blue digital numbers (DN_B), each of which can range from 0 to 255. Therefore, the timing of leaf-flush, leaf-coloring, and leaf-fall can be determined quantitatively by examining time series of proportions of DN_R, DN_G, and DN_B values as percentages of total DN (denoted as %R, %G, %B, respectively) and a vegetation index based on average DN_R, DN_G, and DN_B values, such as the green excess index (denoted as GEI; Richardson et al. 2007) in the region of interest.

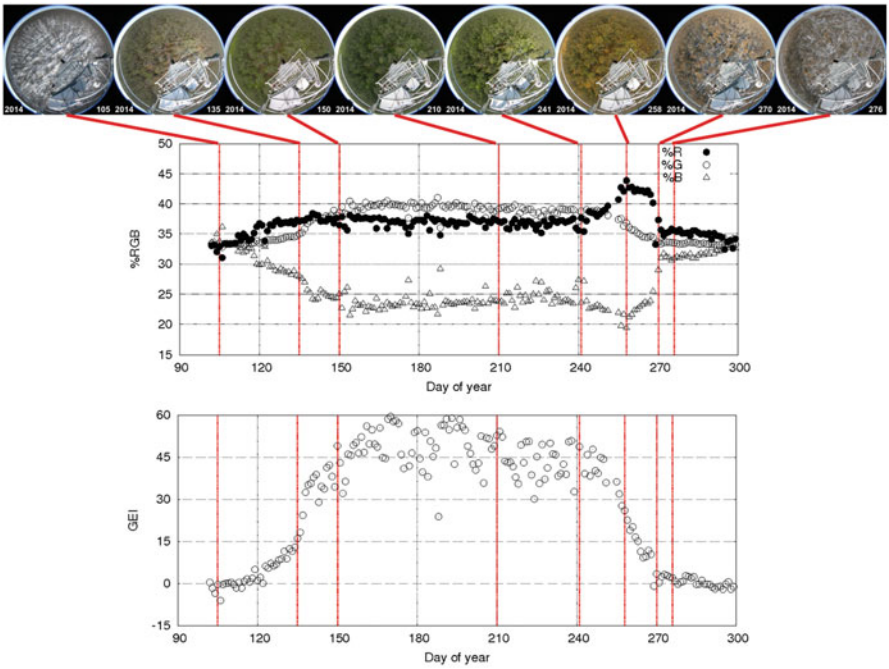

Fig. 10.10 Seasonal changes in %R, %G, %B (upper graph), and GEI (lower graph) from April to October 2014 along with typical phenological images of the Spasskaya Pad larch forest (SSP). Date and day of year (in parenthesis) are shown on each phenological image

$$\%\mathrm{R} = \mathrm{DN_R}/(\mathrm{DN_R} + \mathrm{DN_G} + \mathrm{DN_B}) \tag{10.1}$$

$$\%\mathrm{G} = \mathrm{DN_G}/(\mathrm{DN_R} + \mathrm{DN_G} + \mathrm{DN_B}) \tag{10.2}$$

$$\%\mathrm{B} = \mathrm{DN_B}/(\mathrm{DN_R} + \mathrm{DN_G} + \mathrm{DN_B}) \tag{10.3}$$

$$\mathrm{GEI} = (\mathrm{DN_G} - \mathrm{DN_R}) + (\mathrm{DN_G} - \mathrm{DN_B}) \tag{10.4}$$

Among ecosystems and tree species, %R, %G, %B, and GEI show characteristic seasonal patterns (Nagai et al. 2011; Wingate et al. 2015). At the Spasskaya Pad site in 2014 (Fig. 10.10), %G increased during leaf-flush (DOY 135–150), but %B decreased rapidly. During leaf-coloring and leaf-fall (DOY 240–270), %G decreased. In contrast, %R first increased just before the leaf-coloring peak (DOY 258), after which %R fell steeply, while %B increased rapidly. The GEI time series was characterized by a rapid increase during leaf-flush and a rapid decrease during leaf-coloring and leaf-fall.

By selecting suitable threshold values of %R, %G, %B, and GEI, it is possible to detect year-to-year variations in the timing of leaf-flush, leaf-coloring, and leaf-fall. For example, Nagai et al. (2013) developed a statistical phenological model for estimating the timing of leaf-flush and leaf-fall in a deciduous broad-leaved forest in Japan by examining the relationship between leaf-flush and leaf-fall dates

determined from daily phenological images and daily mean air temperature. The development of a statistical phenological model, based on observations obtained with time-lapse digital cameras at multiple field sites, would be useful for estimating leaf-flush and leaf-fall dates in eastern Siberia and for characterizing their spatial distribution along a latitudinal gradient. Toward this aim, inexpensive, battery-driven time-lapse digital cameras (e.g., Garden Watch Cam, Brinno, Taiwan) have been installed at multiple field sites in Alaska (Kobayashi et al. 2016).

10.4.4 Integrating In Situ and Satellite Observations

Long-term continuous phenological images allow testing and validation of the timing of SGS and EGS values determined by using satellite-observed vegetation indices. In NDVI and enhanced vegetation index (EVI), where $EVI = G \times \{(NIR - red)/[NIR + (C1 \times red) - (C2 \times blue) + L]\}$ ($G = 2.5$, $C1 = 6$, $C2 = 7.5$, and $L = 1$ are constants; Huete et al. 2002), analyses, it is more difficult to determine the timing of EGS than of SGS, because the timing and spatial patterns of leaf-coloring and leaf-fall vary among tree species (Nagai et al. 2010, 2014).

The green–red vegetation index (GRVI), where GRVI = (green – red)/(green + red) (Tucker 1979; Motohka et al. 2010), which is based only on seasonal changes in the color of the canopy, is more suitable for determining the timing of EGS in deciduous broad-leaved forests than either NDVI or EVI (Nagai et al. 2014). Before leaf-flush begins in spring, GRVI shows negative values, and it again becomes negative values after the peak of leaf-coloring and leaf-fall in autumn (Motohka et al. 2010; Nagai et al. 2014).

At the Spasskaya Pad site (Fig. 10.11), the first date in each year from 2003 to 2015 on which $GRVI_{MODIS}$ was more than or equal to zero in spring corresponded to the beginning of leaf-flush in larch, whereas the first date on which $GRVI_{MODIS}$ was less than zero in autumn corresponded to the peak of leaf-coloring in birch, which was earlier than the leaf-coloring peak in larch. These results indicate that $GRVI_{MODIS} = 0$ is a useful criterion for detecting both the start and end of the functional growing season (i.e., duration of photosynthetic capacity) in larch forests in eastern Siberia.

Using these ground-truthing data, we analyzed the spatial distribution of the first dates on which $GRVI_{MODIS}$ was more than or equal to zero in spring and the first dates on which it was less than zero in autumn in 2015 for the whole of eastern Siberia (Fig. 10.12). The timing of SGS was earlier at low latitudes and elevations than at high latitudes and elevations. In contrast, the timing of EGS was later at low latitudes and elevations than at high latitudes and elevations. A similar analysis for the period from 2003 to 2015 revealed the spatial characteristics of the year-to-year variability in the timing of SGS and EGS (not shown). Analyses of the relationships among year-to-year variability in the timing of SGS and EGS, PFT, aboveground biomass, topography, and latitudinal gradients in eastern Siberia might allow the sensitivity and vulnerability of plant phenology to climate change to be evaluated.

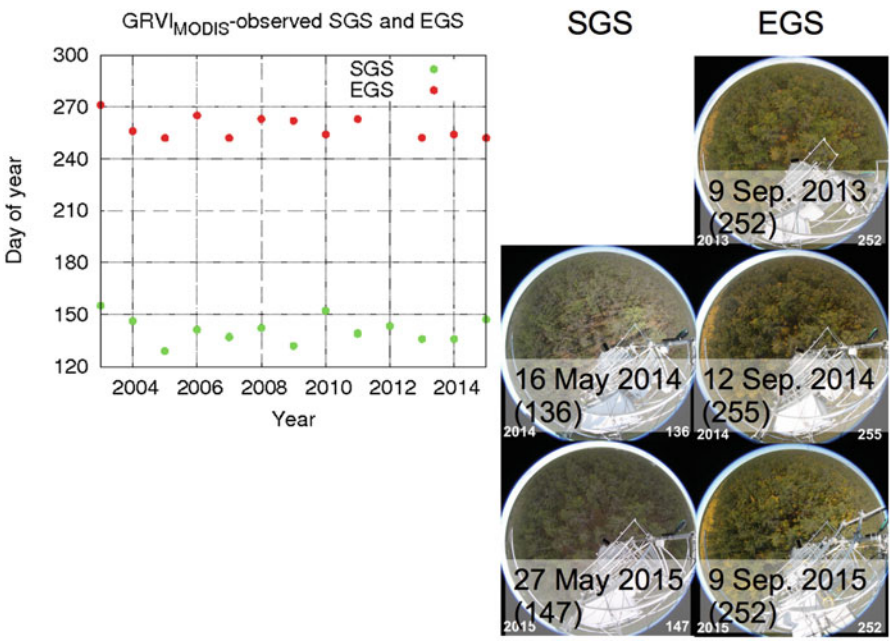

Fig. 10.11 Year-to-year variability in SGS and EGS (day of year, DOY), based on GRVI observed by Terra/Aqua-MODIS (GRVI$_{MODIS}$), in the Spasskaya Pad larch forest, along with phenological images obtained on the first date on which GRVI$_{MODIS}$ was more than or equal to zero in spring (SGS) and the first date on which it less than zero in autumn (EGS). We substituted the canopy surface image on 12 September 2014 for the missing image on 11 September 2014. EGS in 2012 was missing

10.5 Concluding Remarks

In this chapter, we summarized the usefulness and uncertainties of remote-sensing techniques to monitor the spatiotemporal variability of aboveground biomass, PFT, and growing season duration in eastern Siberia by refereeing previous studies and introducing our own developed studies. To increase our understanding of interactions between terrestrial ecosystems and the atmosphere in eastern Siberia, the following three challenging tasks should be undertaken.

The spatiotemporal variability of the aboveground biomass and growing season duration detected by remote-sensing observations are important for evaluating photosynthetic capacity. However, this information cannot be used to evaluate photosynthetic activity directly. One remote-sensing technique that allows their activities to be directly evaluated is the measurement of the fluorescent intensity of chlorophyll. Solar-induced chlorophyll fluorescence is being observed by the thermal and NIR sensor for carbon observation–Fourier transform spectrometer sensor onboard Japan's Greenhouse Gases Observing Satellite (GOSAT) (Frankenberg et al. 2011).

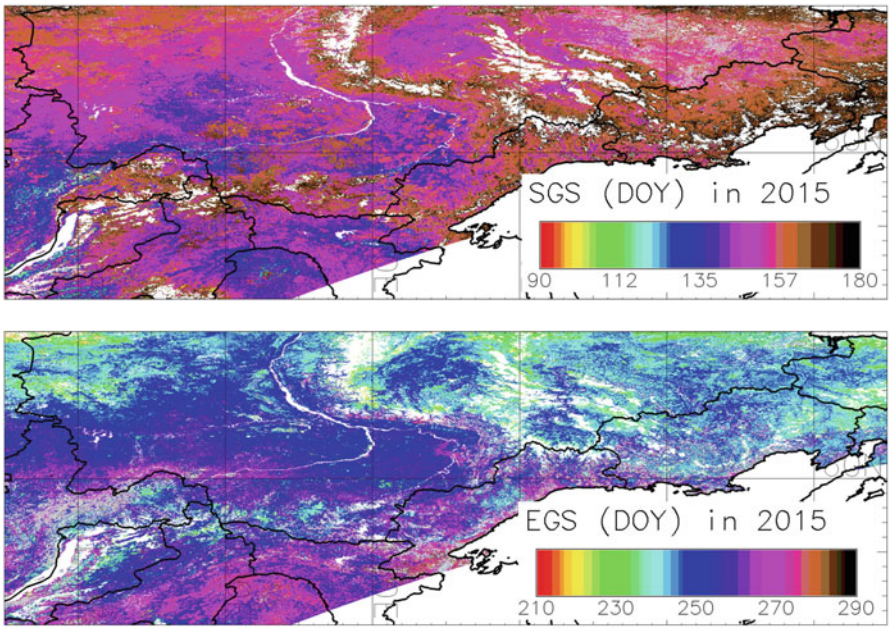

Fig. 10.12 Spatial distribution of the first date on which $GRVI_{MODIS}$ was more than zero in spring (i.e., SGS; top) and the first date on which $GRVI_{MODIS}$ was less than zero in autumn (i.e., EGS; bottom) in 2015 in eastern Siberia between 70°N and 50°N and 105°E and 165°E. The color scales show day of year (DOY)

To accurately detect the degradation of forests, the transition of forested areas to bogs, and the expansion of alases in eastern Siberia, analyses of satellite data with a high spatial resolution, such as data acquired by the AVNIR-2 (Advances Visible and Near Infrared Radiometer type 2) sensor onboard ALOS (spatial resolution, 10 m) or the WorldView-3 satellite (spatial resolution, 1.24 m), are required. Satellite observations by SAR, such as PALSAR-2 onboard ALOS-2, which are not affected by atmospheric noise or cloud contamination and have a spatial resolution of 3–10 m, are also useful for this purpose.

Ecosystem ecotones such as that between forest and tundra are considered to be highly sensitive and vulnerable to climate change, but ground-truthing of high-latitude ecotones is still insufficient. At the Kodac site near Chokurdakh in the northern part of eastern Siberia (70°33′47”N, 148°15′49″E), CO_2 fluxes have been measured, and phenological observations have been made by using inexpensive battery-powered time-lapse cameras since 2013. Further field studies at additional ecosystem ecotone sites are needed for the validation and testing of satellite remote-sensing observations.

References

Buitenwerf R, Rose L, Higgins SI (2015) Three decades of multi-dimensional change in global leaf phenology. Nat Clim Chang 5:364–368

Delbart N, Le Toan T, Kergoat L, Fedotova V (2006) Remote sensing of spring phenology in boreal regions: a free of snow-effect method using NOAA–AVHRR and SPOT–VGT data (1982–2004). Remote Sens Environ 101:52–62

Flessa H, Rodionov A, Guggenberger G, Fuchs H, Magdon P, Shibistova O, Zrazhevskaya G, Mikheyeva N, Kasansky OA, Blodau C (2008) Landscape controls of CH_4 fluxes in a catchment of the forest tundra ecotone in northern Siberia. Glob Chang Biol 14:2040–2056

Frankenberg C, Butz A, Toon GC (2011) Disentangling chlorophyll fluorescence from atmospheric scattering effects in O-2 A-band spectra of reflected sun-light. Geophys Res Lett 38:L03801. https://doi.org/10.1029/2010GL045896

Giglio L, Randerson JT, Werf GR (2013) Analysis of daily, monthly, and annual burned area using the fourth-generation global fire emissions database (GFED4). J Geophys Res Biogeo 118 (1):317–328

Huete A, Didan K, Miura T, Rodriguez EP, Gao X, Ferreira LG (2002) Overview of the radiometric and biophysical performance of the MODIS vegetation indices. Remote Sens Environ 83:195–213

Iida SI, Ohta T, Matsumoto K, Nakai T, Kuwada T, Kononov AV et al (2009) Evapotranspiration from understory vegetation in an eastern Siberian boreal larch forest. Agric For Meteorol 149 (6):1129–1139

Iijima Y, Ohta T, Kotani A, Fedorov AN, Kodama Y, Maximov TC (2014) Sap flow changes in relation to permafrost degradation under increasing precipitation in an eastern Siberian larch forest. Ecohydrology 7:177–187

James ME, Kalluri SN (1994) The Pathfinder AVHRR land data set: an improved coarse resolution data set for terrestrial monitoring. Int J Remote Sens 15(17):3347–3363

Jin M, Treadon RE (2003) Correcting the orbit drift effect on AVHRR land surface skin temperature measurements. Int J Remote Sens 20:4543–4558

Kajimoto T, Matsuura Y, Sofronov MA, Volokitina AV, Mori S, Osawa A, Abaimov AP (1999) Above- and belowground biomass and net primary productivity of a *Larix gmelinii* stand near Tura, Central Siberia. Tree Physiol 19:815–822

Kajimoto T, Matsuura Y, Osawa A, Abaimov AP, Zyryanova OA, Isaev AP, Yefremov DP, Mori S, Koike T (2006) Size-mass allometry and biomass allocation of two larch species growing on the continuous permafrost region in Siberia. For Ecol Manag 222:314–325

Knyazikhin Y, Martonchik JV, Myneni RB, Diner DJ, Running SW (1998) Synergistic algorithm for estimating vegetation canopy leaf area index and fraction of absorbed photosynthetically active radiation from MODIS and MISR data. J Geophys Res 103(D24):32257

Kobayashi H, Suzuki R, Kobayashi S (2007) Reflectance seasonality and its relation to the canopy leaf area index in an eastern Siberian larch forest: multi-satellite data and radiative transfer analyses. Remote Sens Environ 106(2):238–252

Kobayashi H, Delbart N, Suzuki R, Kushida K (2010) A satellite-based method for monitoring seasonality in the overstory leaf area index of Siberian larch forest. J Geophys Res Biogeo 115: G01002. https://doi.org/10.1029/2009JG000939

Kobayashi H, Yunus AP, Nagai S, Sugiura K, Kim Y, Van Dam B, Nagano H, Zona D, Harazono Y, Bret-Harte MS, Ichii K, Ikawa H, Iwata H, Oechel WC, Ueyama M, Suzuki R (2016) Latitudinal gradient of spruce forest understory and tundra phenology in Alaska as observed from satellite and ground-based data. Remote Sens Environ 177:160–170

Kushida K, Isaev AP, Maximov TC, Takao G, Fukuda M (2007) Remote sensing of upper canopy leaf area index and forest floor vegetation cover as indicators of net primary productivity in a Siberian larch forest. J Geophys Res Biogeo 112(112):G02003. https://doi.org/10.1029/2006JG000269

Liu Y, Liu R, Pisek J, Chen JM (2017) Separating overstory and understory leaf area indices for global needleleaf and deciduous broadleaf forests by fusion of MODIS and MISR data. Biogeosciences 14(5):1093

Motohka T, Nasahara KN, Oguma H, Tsuchida S (2010) Applicability of green–red vegetation index for remote sensing of vegetation phenology. Remote Sens 2:2369–2387

Motohka T, Nasahara KN, Murakami K, Nagai S (2011) Evaluation of sub-pixel cloud noises on MODIS daily spectral indices based on in situ measurements. Remote Sens 3:1644–1662

Myneni RB, Keeling CD, Tucker CJ, Asrar G, Nemani RR (1997a) Increased plant growth in the northern high latitudes from 1981 to 1991. Nature 386(6626):698

Myneni RB, Nemani RR, Running SW (1997b) Estimation of global leaf area index and absorbed PAR using radiative transfer models. IEEE Trans Geosci Remote Sens 35(6):1380–1393

Myneni RB, Dong J, Tucker CJ, Kaufmann RK, Kauppi PE, Liski J, Zhou L, Alexeyev V, Hughes MK (2001) A large carbon sink in the woody biomass of northern forests. Proc Nat Acad Sci USA 98(26):14784–14789

Myneni RB, Hoffman S, Knyazikhin Y, Privette JL, Glassy J, Tian Y, Wang Y, Song X, Zhang Y, Smith GR, Lotsch A (2002) Global products of vegetation leaf area and fraction absorbed PAR from year one of MODIS data. Remote Sens Environ 83(1):214–231

Nagai S, Nasahara KN, Muraoka H, Akiyama T, Tsuchida S (2010) Field experiments to test the use of the normalized difference vegetation index for phenology detection. Agric For Meteorol 150:152–160

Nagai S, Maeda T, Gamo M, Muraoka H, Suzuki R, Nasahara KN (2011) Using digital camera images to detect canopy condition of deciduous broad-leaved trees. Plant Ecol Diver 4:78–88

Nagai S, Saitoh TM, Kurumado K, Tamagawa I, Kobayashi K, Inoue T, Suzuki R, Gamo M, Muraoka H, Nasahara KN (2013) Detection of bio-meteorological year-to-year variation by using digital canopy surface images of a deciduous broad-leaved forest. SOLA 9:106–110

Nagai S, Inoue T, Ohtsuka T, Kobayashi H, Kurumado K, Muraoka H, Nasahara KN (2014) Relationship between spatio-temporal characteristics of leaf-fall phenology and seasonal variations in near surface- and satellite-observed vegetation indices in a cool-temperate deciduous broad-leaved forest in Japan. Int J Remote Sens 35:3520–3536

Nagai S, Akitsu T et al (2018) 8 million phenological and sky images from 29 ecosystems from the Arctic to the tropics: the Phenological eyes network. Ecol Res 33(6):1091. https://doi.org/10.1007/s11284-018-1633-x

Nasahara KN, Nagai S (2015) Review: development of an in-situ observation network for terrestrial ecological remote sensing—the Phenological eyes network (PEN). Ecol Res 30:211–223

Piao S, Wang X, Ciais P, Zhu B, Wang TAO, Liu JIE (2011) Changes in satellite-derived vegetation growth trend in temperate and boreal Eurasia from 1982 to 2006. Glob Chang Biol 17 (10):3228–3239

Pinzon JE, Tucker CJ (2014) A non-stationary 1981-2012 AVHRR NDVI3g time series. Remote Sens 6(8):6929–6960

Prentice IC, Cramer W, Harrison SP, Leemans R, Monserud RA, Solomon AM (1992) A global biome model based on plant physiology and dominance, soil properties and climate. J Biogeogr 19:117–134

Richardson AD, Jenkins JP, Braswell BH, Hollinger DY, Ollinger SV, Smith M-L (2007) Use of digital webcam images to track spring green-up in a deciduous broadleaf forest. Oecologia 152:323–334

Richardson AD, Keenan TF, Migliavacca M, Ryu Y, Sonnentag O, Toomey M (2013) Climate change, phenology, and phenological control of vegetation feedbacks to the climate system. Agri Forest Meteorol 169:156–173

Sato H, Kobayashi H, Iwahana G, Ohta T (2016) Endurance of larch forest ecosystems in eastern Siberia under warming trends. Ecol Evol 6(16):5690–5704

Simard M, Pinto N, Fisher JB, Baccini A (2011) Mapping forest canopy height globally with spaceborne lidar. J Geophys Res 116:G04021. https://doi.org/10.1029/2011JG001708

Suzuki R, Nomaki T, Yasunari T (2001) Spatial distribution and its seasonality of satellite-derived vegetation index (NDVI) and climate in Siberia. Int J Climatol 21:1321–1335

Suzuki R, Hiyama T, Asanuma J, Ohata T (2004) Land surface identification near Yakutsk in eastern Siberia using video images taken from a hedgehopping aircraft. Int J Remote Sens 25 (19):4015–4028

Suzuki R, Masuda K, Dye DG (2007) Interannual covariability between actual evapotranspiration and PAL and GIMMS NDVIs of northern Asia. Remote Sens Environ 106:387–398

Tucker CJ (1979) Red and photographic infrared linear combinations for monitoring vegetation. Remote Sens Environ 8:127–150

Wingate L, Ogée J, Cremonese E, Filippa G, Mizunuma T, Migliavacca M et al (2015) Interpreting canopy development and physiology using a European phenology camera network at flux sites. Biogeosciences 12:5995–6015

Wright IJ, Reich PB, Westoby M, Ackerly DD, Baruch Z, Bongers F et al (2004) The worldwide leaf economics spectrum. Nature 428:821–827

Zhou L, Tucker CJ, Kaufmann RK, Slayback D, Shabanov NV, Myneni RB (2001) Variations in northern vegetation activity inferred from satellite data of vegetation index during 1981 to 1999. J Geophys Res Atmos 106(D17):20069–20083